Bioactive Materials 10 (2022) 430–442

Contents lists available at ScienceDirect

Bioactive Materials

journal homepage: www.sciencedirect.com/journal/bioactive-materials

Chitosan coatings with distinct innate immune bioactivities differentially stimulate angiogenesis, osteogenesis and chondrogenesis in poly-caprolactone scaffolds with controlled interconnecting pore size

Caroline D. Hoemann [a,b,*], Javier Rodríguez González [a], Jessica Guzmán-Morales [a], Gaoping Chen [a], Ebrahim Jalali Dil [a,c], Basil D. Favis [a,c]

[a] Department of Chemical Engineering, Polytechnique Montreal, QC, Canada
[b] Department of Bioengineering George Mason University, VA, USA
[c] Centre de Recherche sur les Systèmes Polymères et Composites à Haute Performance (CREPEC), Canada

ARTICLE INFO

Keywords:
Bone tissue engineering
Cartilage tissue engineering
Hematoma
Chitosan
Angiogenesis
Osteogenesis
Inflammation

ABSTRACT

This study tested whether osseous integration into poly (ε-caprolactone) (PCL) bioplastic scaffolds with fully-interconnecting 155 ± 8 μm pores is enhanced by an adhesive, non-inflammatory 99% degree of deacetylation (DDA) chitosan coating (99-PCL), or further incorporation of pro-inflammatory 83% DDA chitosan microparticles (83-99-PCL) to accelerate angiogenesis. New Zealand White rabbit osteochondral knee defects were press-fit with PCL, 99-PCL, 83-99-PCL, or allowed to bleed (drill-only). Between day 1 and 6 weeks of repair, drill-only defects repaired by endochondral ossification, with an 8-fold higher bone volume fraction (BVF) versus initial defects, compared to a 2-fold (99-PCL), 1.1-fold (PCL), or 0.4-fold (83-99-PCL) change in BVF. Hematoma innate immune cells swarmed to 83-99-PCL, elicited angiogenesis throughout the pores and induced slight bone resorption. PCL and 99-PCL pores were variably filled with cartilage or avascular mesenchyme near the bone plate, or angiogenic mesenchyme into which repairing trabecular bone infiltrated up to 1 mm deep. More repair cartilage covered the 99-PCL scaffold (65%) than PCL (18%) or 83-99-PCL (0%) ($p < 0.005$). We report the novel finding that non-inflammatory chitosan coatings promoted cartilage infiltration into and over a bioplastic scaffold, and were compatible with trabecular bone integration. This study also revealed that *in vitro* osteogenesis assays have limited ability to predict osseous integration into porous scaffolds, because (1) *in vivo,* woven bone integrates from the leading edge of regenerating trabecular bone and not from mesenchymal cells adhering to scaffold surfaces, and (2) bioactive coatings that attract inflammatory cells induce bone resorption.

1. Introduction

Bone tissue engineering (BTE) strategies aim to control polymer structures and bioactivities to favor bone growth into a porous scaffold [1]. Although much progress has been gained in structural design, a persisting challenge remains in understanding how to guide the inward migration and differentiation of bone marrow cells and blood vessels, to form mineralized tissue deep in a porous scaffold [2]. Poly (ε-caprolactone) (PCL) has received a lot of attention as a biocompatible polymer of choice, partly because the bioplastic can be melted to form different shapes that support cell infiltration and osteogenesis by mesenchymal stem cells (MSCs) *in vitro* [3–8], and permit woven bone deposition *in vivo* (with the help of exogenous cells or bioactive factors) [9–11]. Pore size has been studied as a factor that influences osseous integration into different materials *in vivo*. Scaffolds with pore diameters ≤100 μm showed limited vascularization [12] while promoting chondrogenesis [13]. Vascular bone will spontaneously infiltrate into scaffolds with >100 μm–850 μm pores but usually only the outer pores [9,11,14–16].

Previous collaborative works developed PCL scaffolds with fully-interconnected pores and precise pore sizes to evaluate their potential

Peer review under responsibility of KeAi Communications Co., Ltd.

* Corresponding author. Department of Bioengineering, Institute for Advanced Biomedical Research, George Mason University, 10920 George Mason Circle, Manassas, VA, 20110, USA.

E-mail addresses: choemann@gmu.edu (C.D. Hoemann), javier.rodriguezgonzalez@mail.mcgill.ca (J. Rodríguez González), jgm1409@yahoo.com.mx (J. Guzmán-Morales), gaopingchen@gmail.com (G. Chen), ebrahim.jalalidil@polymtl.ca (E. Jalali Dil), basil.favis@polymtl.ca (B.D. Favis).

https://doi.org/10.1016/j.bioactmat.2021.09.012
Received 1 July 2021; Received in revised form 6 September 2021; Accepted 6 September 2021
Available online 16 September 2021
2452-199X/© 2021 The Authors. Publishing services by Elsevier B.V. on behalf of KeAi Communications Co. Ltd. This is an open access article under the CC BY-NC-ND license (http://creativecommons.org/licenses/by-nc-nd/4.0/).

in BTE applications [7,8,17,18]. These scaffolds were formed by melt-blending PCL with poly (ethylene oxide) (PEO) at the co-continuous composition (where both phases form a 3-dimensional interpenetrated network) [17]. After melt-blending, a static annealing step and annealing time (0.5–3 h) is used to control the phase size in the polymer blend, then cooling and extraction of the porogen phase (PEO) transforms PCL into a porous scaffold. This approach was used to generate scaffolds with 84, 116, 141, and 162 μm average pore diameter with smooth concave interconnecting surfaces that resemble a trabecular network [17]. PCL has hydrophobic surfaces that inhibit cell attachment, which is needed for *in vitro* osteogenesis [5,19]. Therefore a method was worked out to coat the PCL scaffold pore surfaces with hydrophilic cationic materials [7,8]. This was achieved through the Layer-by-Layer (LbL) self-assembly of polyelectrolytes (poly (diallyldimethylammonium chloride, PDADMAC, as polycation and poly (sodium 4-styrenesulfonate), PSS as polyanion), using the last anionic PSS layer to capture a uniform coating of cationic chitosan as the final outside layer. This approach transformed a porous hydrophobic polymer material of highly controlled morphology to one with essentially complete chitosan-like surface characteristics. Human bone marrow-derived mesenchymal stem cells (MSCs) infiltrating the PCL pores produced more mineralized matrix in 3-D *in vitro* osteogenesis assays when the PCL scaffold was coated with 99% degree of deacetylation (DDA) chitosan [7,8]. Based on these promising results, the purpose of this study was to evaluate the effect of a 99% DDA chitosan coating on *in vivo* osteogenesis in the PCL scaffold, using an established skeletally mature rabbit model of osteochondral repair [20].

Prior to initiating this study we were aware that a variety of scaffolds or hydrogels were previously implanted in osteochondral defects, and either failed to incorporate any tissue, leaving a bone void, or formed tissues inside the scaffold pores with unknown mineralization state [21–25]. Bone fractures can produce mineralized tissues through two pathways: calcified cartilage (callus) in regions devoid of blood vessels, and woven (lamellar) bone in vascularized areas. Angiogenesis is needed to permit diffusion of nutrients and oxygen (100–300 μm) from capillary beds to actively regenerating woven bone [26,27]. Angiogenic factors or scaffolds pre-seeded with vascular cells were previously used as a means to accelerate angiogenesis [26,27]. In this study, however, we considered that the hematoma is the first tissue to occupy a BTE scaffold after implantation. Recent data showed that structurally distinct chitosans have different innate immune activation potential that could be used to guide bone fracture repair responses [28]. Chitosan is a family of linear polysaccharide polymers with variable glucosamine and *N*-acetyl glucosamine, where the % glucosamine is equal to the % DDA level [29]. Microparticles of 99% DDA chitosan with 10 kDa–30 kDa (but not 130 kDa) were shown to induce anti-inflammatory responses *in vitro* in human macrophages, including the release of interferon alpha and interleukin-1 receptor antagonist (IL-1ra) [28]. We therefore used 99% DDA 10 kDa chitosan to coat the PCL scaffold for its cell-adhesive, non-inflammatory and potentially anti-inflammatory activity *in vivo*. By contrast, ~80% DDA chitosan microparticles (but not ≥95% DDA microparticles) when incorporated into a hematoma specifically attracted neutrophils and macrophages and stimulated angiogenesis [30–32]. These data led us to hypothesize that the pro-inflammatory activities of 83% DDA chitosan microparticles could be used to draw angiogenic blood vessels into PCL pores coated with 99% DDA chitosan, and thereby promote woven bone ingrowth. We implanted the PCL scaffolds by press-fitting into epiphyseal microdrill defects to test the hypothesis that PCL scaffolds with fully-interconnecting pores undergo more osseous integration *in vivo* when coated with 99% DDA chitosan, and more angiogenesis and osteogenesis when coated with 99% DDA chitosan with added 83% DDA chitosan microparticles. Drill-only defects served as controls for spontaneous repair. For this proof-of-concept study we analyzed initial defects and repair tissues in 6 osteochondral defects per condition at 6 weeks post-surgery, when osteochondral mineralization processes were expected to be on-going.

2. Materials and methods

2.1. Materials

Commercial-grade PCL (CAPA 6800, 80 kDa) was purchased from Solvay (Brussels, Belgium). Poly (ethylene) oxide (PEO) water-soluble polymer (POLYOX™ WSR-N10, 100 kDa) was supplied by Dow (Midland, MI). PSS, M_w 70,000, 30 wt % in H_2O, and PDADMAC, M_w 100,000–200,000, 20 wt % in H_2O (#409014), were purchased from Sigma (Oakville, ON, Canada). Chitosan was deacetylated and nitrous acid-depolymerized in-house from starting material (Marinard, NB, Canada) to generate 99% DDA, M_w 9 kDa and 83% DDA, M_w 11 kDa, using NMR spectroscopy to characterize DDA, and gel permeation chromatography to determine M_w[28]. Rhodamine B isothiocyanate–chitosan (RITC-chitosan) derivatives were produced at 1% mol RITC/mol chitosan with 99% DDA, M_w 9 kDa, and 83% DDA, M_w 11 kDa [28]. Hoechst 33258 (H1398) was from Molecular Probes, Safranin O (S2255), fast green (F7252), and hematoxylin (HHS32) were from Sigma (Oakville, ON, Canada).

2.2. PCL scaffold fabrication

PEO/PCL blend preparation and annealing were carried out as described [17] with minor modifications. Briefly, PEO and PCL were dried under vacuum at 40 °C overnight, and blended at 45 vol % PCL/55 vol % PEO ratio in a Brabender internal batch mixer (Plastico, DDR501) at 100 °C, 60 rpm, for 10 min under a nitrogen blanket then quenched in liquid nitrogen. Samples were annealed at 160 °C for 1.5, 2 or 2.5 h in a hot press machine under a nitrogen atmosphere then frozen in liquid nitrogen. Using a mechanical punch, 3 mm diameter, 1.5–2 mm thick discs were cut. PEO was extracted for 7 days with ddH_20 under agitation at room temperature and twice refreshing the rinse water.

2.3. Field emission scanning electron microscopy (FE-SEM)

In order to determine the average pore size of annealed scaffolds, samples were cut using a microtome machine equipped with a cryochamber (Leica-Jung RM 2165). PEO then was extracted using the same procedure as mentioned above. Samples were sputter-coated with a 15 nm thick gold layer, and imaged with an LEI detector by FE-SEM (JSM 7600F, JEOL, acceleration voltage 5 kV, working distance 7 mm). An image analysis software (SigmaScan Pro V5, SigmaPlot) was used to calculate the volume average pore size from 50 pore measures per sample. The diameter of individual pores (d_i) was determined by the software from the pore area (A_i) using Equation (1). Then the software calculated the volume average diameter (d_v) for a given number of pores (n_i) using Equation (2).

$$d_i = \sqrt{\frac{4A_i}{\pi}} \tag{1}$$

$$d_v = \frac{\sum n_i d_i^4}{\sum n_i d_i^3} \tag{2}$$

2.4. Surface modification of PCL scaffolds via LbL deposition of polyelectrolytes and chitosan

In a laminar flow hood, PCL scaffolds were soaked in 45 mL of each solution under static conditions in 50 mL conical tubes, except for the filter-sterile chitosan solutions which were prepared in sterile microfuge tubes, 0.5 mL (see Fig. S1 for more details). PCL discs with 155 μm pores were made antiseptic by soaking in 70% ethanol for 1 h, rinsed overnight in sterile distilled/deionized, MilliQ-purified water (ddH_2O), then stored aseptically (PCL) or coated by depositing layer-by-layer (LbL) polyelectrolytes followed by chitosan as described [7]. LbL coatings were generated with 10 mg/mL PDADMAC (polycation, pH 8 or pH 2)

and PSS (polyanion, pH 2) in 1 M NaCl. A precursor layer was formed by incubating in PDADMAC (pH 8) for 1 h followed by rinsing in water for 1 h. Subsequent coatings were added by incubating the scaffolds for 1 h in PSS (pH 2) alternating with PDADMAC (pH 2) and rinsing between each polyelectrolyte deposition step in ddH_2O for 1 h to remove unbound material for a total of 8 layers. Negatively charged PSS was the final outer layer. LbL-coated scaffolds were made antiseptic by incubation in 70% ethanol followed by three consecutive 1-h rinses in sterile ddH_2O. Within 24 h of use, LbL-coated scaffolds were incubated 4 h in a filter-sterile 2 mg/mL 99% DDA, 9 kDa chitosan solution pH 4 (in ddH_20 with dilute HCl to achieve 95% protonation of free glucosamine and ~pH 4, as previously described [33]) then rinsed for 1 h in sterile ddH_2O to produce 99-PCL. 83-99-PCL scaffolds were produced by placing 99-PCL in a solution of 2 mg/mL 83% DDA, 11 kDa chitosan (in ddH_20 with dilute HCl to achieve 95% protonation of free glucosamine). For all *in vitro* studies and the day 1 *in vivo* implant, the 2 mg/mL chitosan solutions were spiked with 0.1 mg/mL structurally-matched fluorescent RITC-chitosan tracer (99% DDA or 83% DDA, 95% protonation in dilute HCl).

2.5. In vitro asymmetric blood clot chemotaxis assay

Peripheral arterial whole blood was drawn aseptically from an adult New Zealand White rabbit, 0.2 mL liquid aliquots deposited into 12 sterile depyrogenated glass vials, then one sterile scaffold (~12 μL volume) was added or not (PCL, 99-PCL, 83-99-PCL, no scaffold, N = 3 per condition). Specimens were cultured for 60 min at 37 °C. Percent clot retraction was determined from gravimetric analysis of extruded serum. CBC-platelet analysis (Vitatech, QC) was normal (5×10^9/mL red blood cells, 313×10^6/mL platelets, 114 g/L hemoglobin, 0.36 hematocrit, 7.5×10^6/mL white blood cells, 19.8% neutrophils, 65.1% lymphocytes, 7.2% monocytes, 1.7% eosinophils, 6.2% basophils). Samples were fixed in 4% paraformaldehyde/100 mM cacodylate (protected from light), carried through graded sucrose, frozen in OCT, and 10 μm cryosections generated through the middle of each scaffold in the clot using the CryoJane tape transfer system (Fig. S2). Sections were stained with SafraninO-Fast green-iron hematoxylin or Hoechst 33258 to label cell nuclei. Nuclei were counted in 10× magnification images of the blood clot at the edge of each scaffold and the middle of each clot (ImageJ) in 2 cryosections from 3 independent samples per condition.

2.6. In vivo osteochondral repair model and histoprocessing

All experiments with animals were carried out under protocols approved by the University of Montreal Animal Care Committee (Protocol 16–100, Polytechnique Montreal Protocol ANI-1516-20) and according to ARRIVE guidelines [34]. Skeletally mature retired breeder rabbits (N = 7, all females due to unavailable male retired breeders, over 10 months old, 4–5 kg, Charles River, St. Constant, QC, Canada) were housed in individual cages. After placing a fentanyl patch for analgesia, each rabbit was anesthetized with ketamine-xylazine, the knees shaved and disinfected, then the rabbit was maintained on 3% isoflurane/8% oxygen while performing small sequential bilateral arthrotomies to create two 3 mm diameter, 2 mm deep osteochondral drill defects in each knee trochlea. Ringer's Lactated saline irrigation was used to keep the site humidified and remove tissue debris. The defect area was scored with a 3 mm biopsy punch, the cartilage shaved with a flat-blade knife, then the subchondral bone drilled with a 2.9 mm diameter stainless steel burr to 2 mm deep, followed by shaping the base with a 1.4 mm diameter burr to create a hole that could fit a rigid cylindrical implant. Rabbits and knees were randomized prior to surgery to 4 conditions to obtain N = 6 osteochondral defects per condition. In 6 rabbits, both holes in each knee were either left to bleed (control) or press-fit with the same condition 3 mm diameter, 1.5–2 mm thick scaffold (PCL, 99-PCL, or 83-99-PCL). Scaffolds were implanted slightly below the bone surface. In one rabbit euthanized 1 day post-surgery, each of the 4 drill holes had one treatment condition (drill-only and PCL, 99-PCL and 83-99-PCL). Incisions were closed in 3 sutured layers. At 1 day (N = 1) or 6 weeks (N = 6) post-operative rabbits were euthanized under anesthesia by pentobarbital intravenous injection. Distal femurs were fixed in 4% paraformaldehyde/100 mM cacodylate pH 7.2, scanned by micro-computed tomography (micro-CT), processed non-decalcified in methyl methacrylate (MMA) and sagittal serial histology sections were collected at the defect edge, mid-point, and middle of the 2 holes. Sections were left unstained for epifluorescence microscopy or deplastified and stained with Goldner's Trichrome, SafraninO-fast green/iron hematoxylin, or von Kossa-Toluidine blue, then digitally scanned at 40× magnification (Nanozoomer, Hamamatsu). Intra-operative bleeding intensity into the defects was estimated from digital images of the surgical site after inserting PCL scaffold and prior to suturing the knees, by threshold measures of red pixel intensity in a region of interest over each drill hole. Post-operative knee inflammation around the arthrotomy site was scored daily for 7 days post-operative then twice a week thereafter as 0 (no inflammation), 1 (slight effusion), 2 (small bump), 3 (medium), 4 (large bump), then the cumulative scores over 6 weeks were averaged for N = 3 knees per condition.

2.7. Micro-computed tomography

Distal femurs were imaged with a Skyscan 1172 instrument (70 kV, 141 μA, pixel size 9 μm, aluminum filter 0.5 mm, frame averaging (3), 0.42° rotation step). 3-D images were reconstructed using NRecon and analyzed by a blinded observer using DataViewer to align each drill hole perpendicular to the z-axis (N = 28). Bone volume density per tissue volume (BV/TV, %) in the defect area was measured in a cylindrical 3-D volume of interest (VOI) 3 mm in diameter and 1.5 mm deep in the drill hole area. CTAn was used to measure the distance from the top to bottom of the hole (drill hole depth). Using DataViewer, a polygonal line tool was used to trace the perimeter of unmineralized residual drill hole area at the top of the hole, −0.5 mm, and −1.5 mm from the top then an inverted threshold was used to obtain the cross-sectional area (residual drill hole area, mm^2) (Fig. S3).

2.8. Quantitative histomorphometry and blood vessel stereology

For the 4 tissue types we analyzed (bone, cartilage, fibrous tissue, blood vessels), we used 3 different histology stains in non-decalcified plastic sections to clearly identify these tissues. Bone and calcified cartilage were identified by green-stained tissue (Goldner's Trichrome) that also stained black with the von Kossa mineral stain, and tissue morphology. Fibrous tissue was identified by a pale green-stained tissue (Goldner's Trichrome) that was not stained black by von Kossa stain. Goldner's Trichrome also stains newly deposited osteoid pink on the surface of green-stained woven bone, and red blood cells are stained red which facilitated identification of blood vessels. Cartilage was identified by cell morphology and a pink/red (SafO), purple (Toluidine blue) or pink/orange/red (Goldner's Trichrome) stained hyaline matrix. Calibrated line measures of % resurfacing with repair cartilage tissue were carried out by a blinded observer using digital scans (NDPview) of 2 distinct Gomori trichrome-stained sections, one collected near the edge and one through the middle of each drill hole. % SafO tissue or % total tissue resurfacing was measured by dividing the length of all SafO + soft tissue or all soft tissue along the defect surface by defect width. % subchondral cartilage was measured in 10× magnification images below the cartilage-bone interface near the edge or in the defect middle using a free-hand draw tool (NDPview) to outline total subchondral cartilage area (mm^2) which was divided by the total scaffold area or drill defect area occupying the 405 mm^2 image. Blood vessel length density (L_v, vessels/mm^2) [32] was measured by scoring all blood vessel cross-sections inside the PCL pore tissue area and divided by total scaffold area, or by 405 mm^2 for drill-only defects.

2.9. Statistical analyses

Differences between groups were analyzed using JMP® Pro (v14.1.0, SAS). 2-tailed Student's t-test was used to analyze clot retraction, leukocyte density and transient knee effusion (N = 3). Analysis of the variance of the mean (ANOVA) with Tukey Honest Significant Differences (HSD) post-hoc was used to analyze the effect of condition on osteochondral defect bleeding (N = 7), and the effect of scaffold on 6-week histological repair using microdrill hole as the experimental unit (N = 6). Response variables (subchondral cartilage area, blood vessel L_v, SafO+ % resurfacing, total tissue % resurfacing) in sections through the defect edge or defect middle at 6 weeks of repair were analyzed according to condition as an explanatory variable (drill-only, PCL, 99-PCL, 83-99-PCL). Micro-CT measures analyzed response variables BV/TV (%), or residual drill cross-sectional area (mm^2) as a between-factor with depth as a within-factor for explanatory variables of condition (day 1 defects: N = 4 drill holes; 6-week repair drill-only, PCL, 99-PCL, 83-99-PCL, N = 6). Significance was set at $p < 0.05$.

3. Results

3.1. PCL scaffold fabrication, chitosan coating, and in vitro blood clot-scaffold interactions

PCL scaffold cylinders with fully interconnected pores were fabricated with a 1.5, 2.0, and 2.5 h static annealing period, to obtain the targeted 155 μm ± 8 μm pore size with a 2 h annealing period (Fig. 1a and b). PCL cylinders, 3 mm in diameter and 2 mm thick, were treated with alternating polyelectrolyte LbL layers followed by 99% DDA chitosan laced with structurally matched chitosan fluorescent tracer (99-PCL). All 99-PCL scaffold surfaces were uniformly coated with 99% DDA chitosan (~1–3 μm thick coating, Fig. 1c). Other 99-PCL scaffolds (without fluorescent tracer) were soaked in dilute 83% DDA chitosan containing 83% DDA RITC-chitosan tracer (83-99-PCL); these scaffolds acquired a uniform 83% DDA chitosan surface coating on top of the 99-PCL surfaces (Fig. 1d). Soluble 83% DDA chitosan was deliberately left in the 83-99-PCL pore spaces in order to produce chitosan microparticles upon contact with liquid whole blood at neutral pH [31,35].

Innate immune cell-scaffold interactions were analyzed in an "asymmetric" clot chemotaxis assay (Figs. 2 and S2). Structurally-matched fluorescent chitosan tracers were used to visualize the chitosan coatings and microparticles in the clots. During 1 h at 37 °C, peripheral blood clot cells "swarmed" to the 83-99-PCL scaffold, as shown by a 2-fold higher cell density at the scaffold perimeter compared to 99-PCL and PCL ($p < 0.05$, Fig. 2a–c). Higher cell density around 83-99-PCL was not explained by greater clot retraction which was similar for the 3 scaffold-clot conditions (Fig. 2d). Red fluorescent phagocytes were detected along the edges of 99-PCL scaffolds and pores but not PCL (Fig. 2e, PCL and 2f, 99-PCL). These data showed that the clot cells could phagocytose part of the 99% DDA chitosan coating. As for the 83% DDA chitosan microparticles, clot cells were seen to ingest fluorescent 83% DDA RITC-chitosan microparticles that diffused up to 600 μm away from the scaffold edge (white arrowheads, Fig. 2g). These chitosan particles were increasingly scavenged by phagocytes as they approached the scaffold, with the most intensely red fluorescent cells occupying the pores and clustered along the 83-99-PCL scaffold perimeter (Fig. 2g, and inset). Altogether, these data showed a selective pro-inflammatory chemotactic response to 83-99-PCL and not 99-PCL or PCL in the hematoma *in vitro*.

3.2. In vivo effect of scaffold on drill hole bleeding, knee effusion, and macroscopic repair

After implanting the scaffolds in bleeding trochlear microdrill holes, subchondral blood infiltrated the PCL pores at different rates that paralleled the defect bleeding intensity (light, medium, heavy), irrespective of chitosan coatings (Fig. 3). At day 1 post-operative all defects contained a hematoma (Fig. 3b). Transient knee effusion was seen starting at day 3 and up to 22 days post-operative in 10 out of 12 arthrotomy sites. Cumulative knee effusion scores were close to 0 for PCL (low or no effusion) and below 20 for other knees (no effusion to moderate swelling) (Fig. 3d). All effusion scores were below 20; scores over 20 were previously associated with catabolic effects on osteochondral repair [20]. After 6 weeks of repair, drill-only defects were covered with

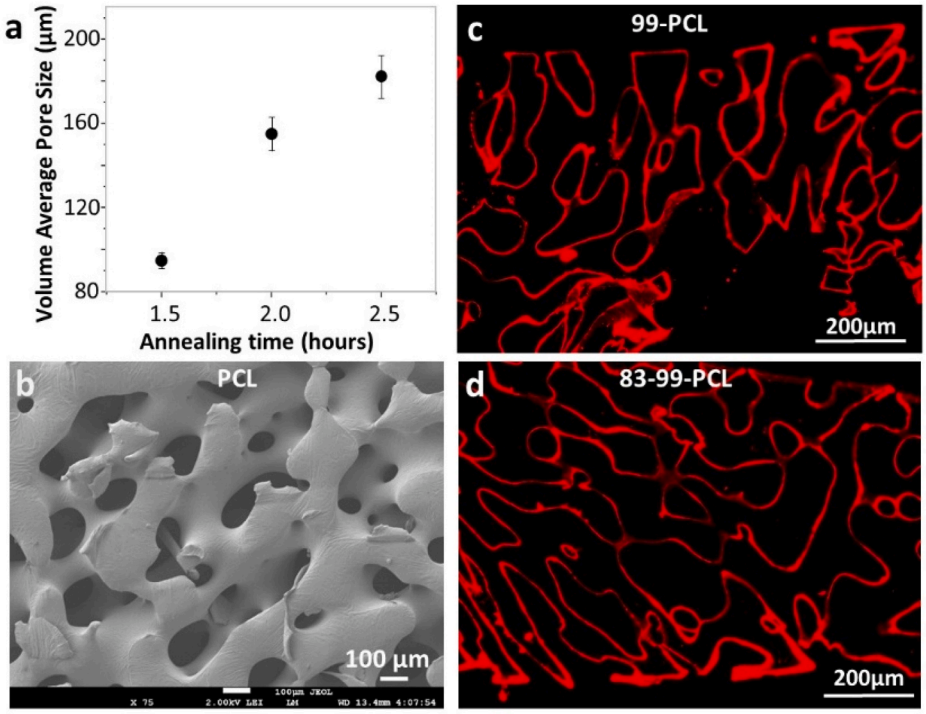

Fig. 1. Fabrication of porous PCL and chitosan coatings. (**a**) Scaffold blends of 45% PCL/55% PEO annealed for 1.5, 2 or 2.5 h yielded average pore sizes of 95 ± 4 μm, 155 ± 8 μm and 182 ± 10 μm, respectively. (**b**) SEM image at 75× magnification of a PCL scaffold with average 155 μm pore diameter. Epifluorescent images of (**c**) 99-PCL (with RITC-99% DDA chitosan tracer) and (**d**) 83-99-PCL (coated with unlabeled 99% DDA chitosan and then 83% DDA chitosan containing RITC-83% DDA chitosan tracer).

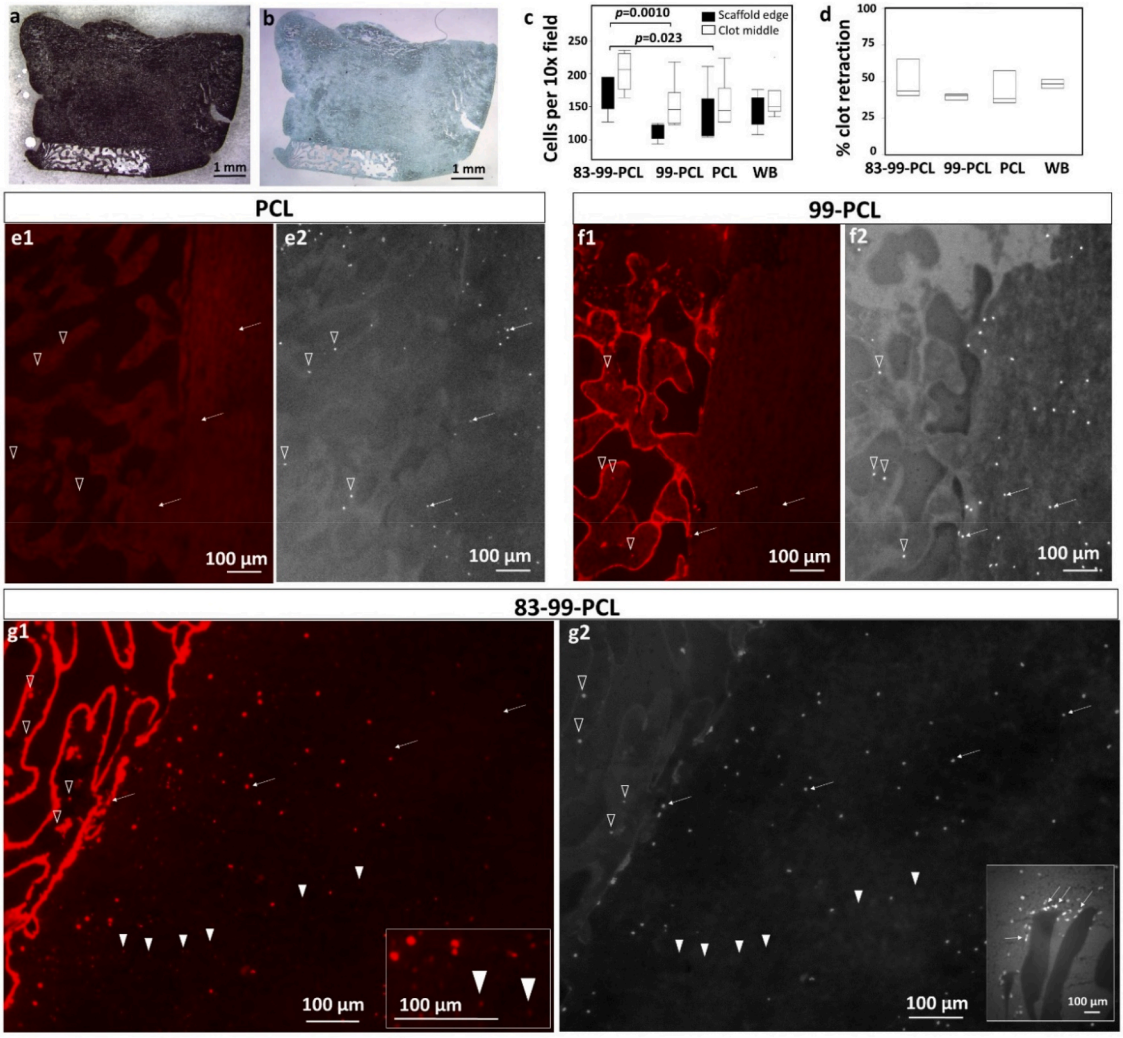

Fig. 2. *In vitro* blood clot-scaffold interactions after 1 h of *in vitro* culture at 37 °C. Rabbit blood clot/scaffold cryosections (**a**) unstained or (**b**) SafraninO/Fast green-stained, (**c**) clot cell density (n = 6) and (**d**) % clot retraction (n = 3). Epifluorescent images of clot samples showing RITC-chitosan (red) and Hoechst 33258-stained cell nuclei (grey scale), for (**e**) PCL/clot, (**f**) 99-PCL/clot and (**g**) 83-99-PCL/clot with chitosan microparticles (arrowheads, **g1** inset), clot cells (arrows, open arrowheads), and cell clusters at the edge (g2, inset). *Symbols:* open triangles: clot cells inside the pores, white arrows: clot cells near the scaffold edge, white arrowheads: 83% DDA chitosan microparticles. Scale bars: (**a,b**) 1 mm, (**c,d**) 200 µm, (**e,f,g**) 100 µm.

a white repair tissue that also covered most of the 99-PCL scaffolds. Many PCL-only and 83-99-PCL implants had exposed scaffold (open arrows, Fig. 3f–h). In 2 knees with exposed PCL-only scaffold, the patellar surface was roughened. Some 83-99-PCL repair tissues had a red hue suggestive of angiogenic blood vessels (thick black arrow, Fig. 3h). Osteophytes were occasionally seen on the outer edges of the distal femur. Synovial fluid in all knees was clear with no signs of effusion and peripheral blood cell counts were normal. After 6 weeks of healing, rabbits were ambulating normally and their knees had no signs of infection.

3.3. *In vivo day 1 hematoma responses to chitosan-coated PCL*

At day 1 post-operative, hematoma filled the drill-only defect, completely filled the pores and partly covered most surfaces of all PCL scaffolds (Figs. 3–5). Chitosan coatings were detected on the PCL scaffold pore surfaces while the 83% DDA chitosan microparticles were displaced to the top of the scaffold clot in the pores, suggesting that the pressure from subchondral bleeding in the direction of the articular cavity pushed the particles up to the bone plate area (red signal, Fig. 4). A hematoma formed in the curved base of the drill hole below 83-99-PCL, 99-PCL, and PCL scaffolds (Fig. 4c and f, Fig. 5, Day 1). In this area, cells were depleted below 83-99-PCL and found instead at the scaffold edges (black arrows, Fig. 4c). Fracture hematoma cells were more evenly distributed below 99-PCL, PCL, and the drill-only defects (Fig. 4f). Phagocytes containing fluorescent RITC-chitosan were observed in and around the 83-99-PCL and 99-PCL scaffolds (white arrows, Fig. 4a, d). These data further supported the hypothesis that 83-99-PCL scaffolds were chemotactic for hematoma phagocytes, and that phagocytes could ingest both chitosan coatings.

3.4. *Chitosan coatings influence chondrogenesis, angiogenesis and osteogenesis in PCL scaffolds*

At 6 weeks post-operative, drill-only defects showed an on-going classical spontaneous endochondral repair response, where a core of calcifying cartilage was undergoing strong vascular bone invasion from the surrounding trabecular bone (Figs. 5, 6a-b). When analyzed as the mean cross-sectional area, drill defects contained on average ~1.2 mm^2 subchondral calcifying cartilage near the defect edge and through the defect middle (Fig. 7a). A predominately cartilaginous tissue was found to infiltrate the pores from the bone plate and variably cover the PCL and 99-PCL scaffolds (Figs. 5 and 6). The morphology of these repair tissues suggested that the cartilage had formed from an outgrowth of MSCs

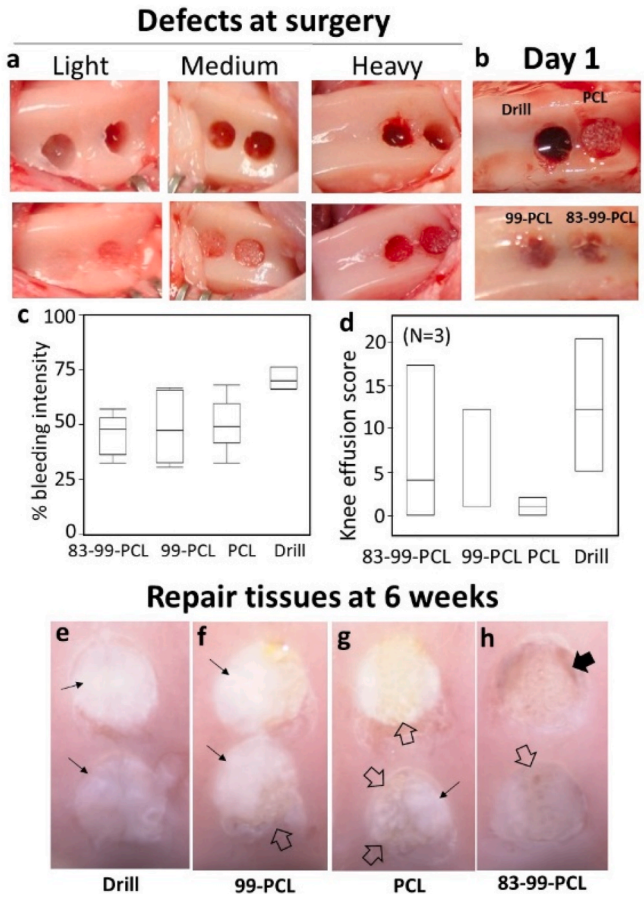

Fig. 3. Osteochondral defect intra-operative bleeding, hematoma formation and transient post-operative knee effusion had minor effects compared to scaffold on macroscopic appearance of 6 week repair tissues. Panels show variable bleeding in drill holes (**a-b**) before and after implanting the scaffolds, (**c**) hematoma formation at day 1, and (**d**) cumulative post-operative knee effusion scores and representative macroscopic appearance of repair tissues for (**e**) 83-99-PCL, (**d**) 99-PCL, (**g**) PCL, (**h**) drill-only. *Symbols* (**e-h**) Thick black arrow: angiogenic tissue; open arrows: exposed PCL bioplastic, thin arrows: cartilage repair tissue.

from immediately adjacent trabecular pores (Figs. S4, S5 & S6). Subchondral cartilage on average infiltrated farther into 99-PCL pores compared to PCL, with an average ~0.6 mm^2 subchondral cartilage in both scaffolds at the edge, and 0.7 mm^2 (99-PCL) or 0.3 mm^2 (PCL) filling pores in the middle of the scaffold (Figs. 5 and 6c-d & 7a). 83-99-PCL scaffold pores were strikingly devoid of cartilage, with 0.2 mm^2 subchondral cartilage at the edge, and 0 mm^2 through the middle of the scaffold ($p < 0.0005$ *vs* drill, $p < 0.05$ *vs* 99-PCL; Figs. 5 and 6f-g & 7a).

A strong angiogenic response to 83-99-PCL was observed, with blood vessels, some very large, surrounding and fully infiltrating the pores throughout the scaffold (red tissue, Figs. 5o, 5, & 6g). One out of six 83-99-PCL scaffolds had persisting sparse inflammatory cells in some pore tissues. Blood vessel length density (L_v) was similar in drill-only and 83-99-PCL defects (15.4/mm^2 *vs* 12.2/mm^2, respectively, Fig. 7b), however blood vessels in drill defects were encased in mineralized tissues (Fig. 6b) whereas blood vessels in 83–99-PCL were enveloped by non-mineralized fibrous tissues or undifferentiated mesenchyme (Fig. 6g1-g2). Drill-only repair tissues and 83-99-PCL pore tissues contained on average two-fold higher blood vessel L_v compared to PCL or 99-PCL (6.5/mm^2 or 6.8/mm^2, respectively, Fig. 7b), but due to variability, the differences were not significant. To summarize, pro-inflammatory 83% DDA chitosan stimulated angiogenesis throughout the PCL scaffold pores and suppressed chondrogenesis and osteogenesis.

SafraninO (SafO)-stained cartilage repair tissue resurfacing the defects was positively correlated with subchondral cartilage area as an explanatory variable (% SafO + cartilage resurfacing = 0.19 + 0.53 × subchondral cartilage area; $R^2 = 0.44$, $p < 0.0001$). In this study, drill-only defects showed excellent SafO-stained cartilage regeneration after 6 weeks of repair. Drill-only defects were covered 100% at the edge and 91.7% over the middle with a hyaline-like cartilage tissue as shown by metachromatic purple Toluidine blue stain, and red SafO stained tissue containing cells with chondrocyte morphology (Figs. 5, 6a and 7c). Less cartilage repair tissue covered scaffolds, with the least cartilage over 83-99-PCL (17%, edge, 0%, middle, $p < 0.0001$ vs drill) and less over the middle of PCL (67% edge, 18% middle, $p < 0.0005$ vs drill, Fig. 7c). The main effect of 99% DDA chitosan was to maintain 3-fold more SafO + cartilage resurfacing over the scaffold middle *vs* PCL-alone (65% vs 18%, $p < 0.05$, Fig. 7c). The effect was partly due to poor soft tissue resurfacing over the middle of the PCL-only scaffold (average 35% *vs* 98% drill, $p < 0.005$, Fig. 7d). Soft tissue covered on average 99% of drill defect surface, 50.8% of the PCL scaffold ($p = 0.004$ *vs* drill), 66.7% of 99-PCL, and 56.7% of 83–99-PCL ($p < 0.05$ *vs* drill) scaffolds.

According to micro-CT measures of mineralized tissue regeneration in the drill holes (Fig. 8), the bone volume fraction of the initial defects (5.6% BV/TV) was significantly increased after 6 weeks of repair in drill-only defects (42% BV/TV, $p < 0.0001$ *vs* all other conditions), slightly higher in defects press-fit with PCL (6.3%) or 99-PCL (10.8%), and lower in 83–99-PCL (2.0%) (Fig. 8f). The initial defect drill hole cross-sectional area was 7.5 mm^2, and narrowed to 3.5 mm^2 at the top and 1 mm^2 at 0.5 mm deep in the trabecular bone in drill-only defects (Fig. 8g). In 6 week-repaired PCL and 99-PCL defects, the residual drill hole area slightly shrank to 6.5 mm^2 and was not significantly different from day 1 defects. By contrast, the 83-99-PCL defects showed a net increase of 1 mm in drill hole cross-sectional area ($p = 0.043$ vs day 1, $p < 0.0005$ vs PCL and 99-PCL, Fig. 8g). Woven bone infiltrated 0.3–1 mm deep into 99-PCL and PCL pores in 4 out of 6 scaffolds, with no clear difference due to 99% DDA chitosan coating. In one out of six 99-PCL treated defects, pore tissues were filled with an angiogenic connective tissue and an extraordinary hyaline cartilage resurfacing over polymer-mesenchymal tissue and not bone (Fig. 5l2 & S4e). Bone marrow-derived cells were detected as adhering along all scaffold pore surfaces (99-PCL, PCL and 83-99-PCL). Therefore, a chitosan coating was not necessary for cells to adhere to the hydrophobic PCL pore surface *in vivo*.

4. Discussion

Results from this study did not support the hypothesis that a 99% DDA chitosan coating is necessary to elicit osteogenesis in PCL scaffold pores *in vivo*. Instead, data showed that repairing fractured trabecular bone infiltrated spontaneously into 155 μm PCL and 99-PCL pores up to 1 mm deep, where angiogenic mesenchyme filled the deeper interconnecting pores. Our study also led to the novel finding that cartilage tissues reproducibly infiltrated superficial PCL pores with a controlled 155 μm pore size. The 99% DDA chitosan coating enhanced pro-chondrogenic mesenchymal cell infiltration, emergence up through the pores, and adhesion of a hyaline-like cartilage tissue to the articular scaffold surface. The data suggested that when cartilage infiltrated deeply into the pores near the articular surface, this led to more complete hyaline-like cartilage resurfacing over the bioplastic, provided that the hydrophobic surface was modified with a cell-adhesive and non-inflammatory 99% DDA chitosan coating. It is possible that the adhesive 99% DDA chitosan coating accelerated mesenchymal progenitor cell migration into the interconnecting pores, but these progenitor cells underwent chondrogenesis instead of osteogenesis. Osteogenesis was only observed at the leading edge of trabecular bone infiltrating from outside the scaffold.

Our results support the hypothesis that 83% DDA chitosan microparticles/coatings stimulate inflammatory angiogenesis throughout the scaffold pores, as this result was obtained in 6 out of 6 defects treated by

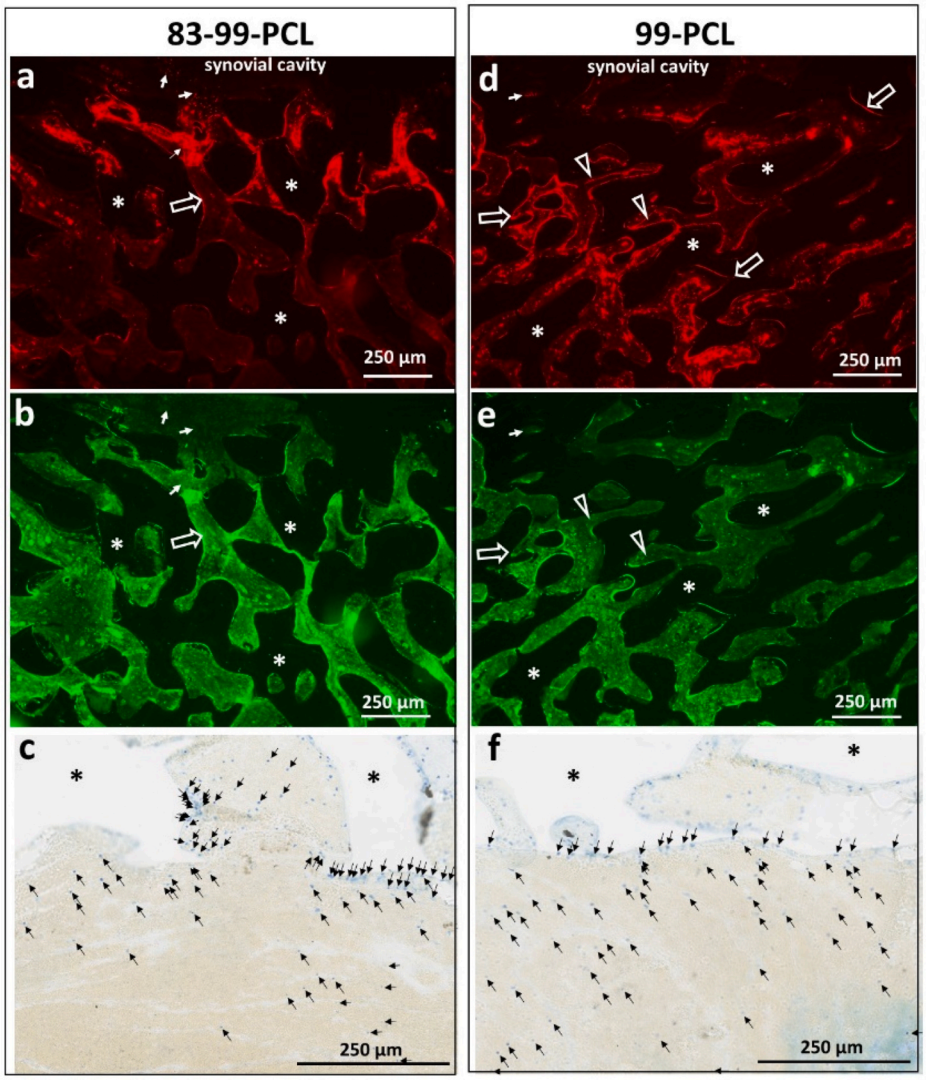

Fig. 4. Hematoma phagocytes swarmed to (**a-c**) 83-99-PCL and not (**d-f**) 99-PCL scaffolds after 1 day *in vivo*. The red signal shows (**a**) 83% DDA or (**d**) 99% DDA chitosan and (**b, e**) matching non-specific green epifluorescence of the hematoma of the same field. Panels (**c & f**) show Toluidine blue/von Kossa stained hematoma below the scaffolds (PCL polymer is indicated by (*) where hematoma cells (blue stain) were displaced towards (**c**) 83-99-PCL and not (**f**) 99-PCL. *Symbols:* (**a,b,d,e**) open arrows: chitosan coating; * = PCL polymer; open arrowheads: detached chitosan coating; thin white arrows: phagocytes with internalized RITC-chitosan; (**c,f**) black arrows: hematoma cells. Scale bars: 250 μm.

83–99-PCL. Inflammatory responses to the small estimated dose of 83% DDA chitosan administered per 83-99-PCL scaffold (10 μg) stimulated angiogenesis, but also induced bone resorption and suppressed chondrogenesis during the 6-week repair period. Although a subchondral angiogenic response elicited by 83% DDA chitosan microparticles showed beneficial effects in microfracture therapy for cartilage repair [20,31,32,36], our new data contra-indicate using inflammatory angiogenesis as a BTE approach in load-bearing bone tissues that require accelerated regeneration of a mechanically stable bone structure. These new data are important to understand, because they highlight certain shortcomings of *in vitro* pass-fail criteria that are traditionally used to develop BTE devices. For example, previous *in vitro* studies suggested that 80%–95% DDA chitosan coatings can be used in BTE applications because they improve mesenchymal stem cell adhesion [6,7]. This notion may seem reasonable based on the results of *in vivo* bone repair studies using chitosans of unknown DDA level [6,37,38]. However this study suggests a risk of bone resorption for chitosans with a deacetylation level ≤85% DDA. This assertion is based on the observation that chitosan microparticles (70% DDA to 85% DDA) [30,39,40] and membranes (56%–81% DDA) [41,42] attract neutrophils, and accumulation of neutrophils or eosinophils in bone can elicit osteoclasts, induce bone remodeling, and delay bone regeneration [20,31,39,40,43]. Although this study used rabbit whole blood, human leukocytes are expected to show the same chemotactic responses [30,42]. Other physical forms of chitosan (soluble oligomers, cross-linked sponges, beads, fibers, hydrogels) could elicit different immunological reactions [29,44]. Future R&D studies could potentially be better informed by analyzing BTE scaffolds for pro-inflammatory responses from innate immune cells *in vitro* as pass-fail criteria (for example using the asymmetric blood clot assay reported here), before progressing to *in vivo* testing. Immunomodulation of the fracture hematoma is a challenging aspect of BTE that deserves more attention. Future studies could test drug-like levels of chitosan (10 ng or less), for example, to elicit angiogenesis without inducing bone resorption.

In this *in vivo* study, endogenous MSCs populated all interconnecting PCL pores. Bone spicules extended from the flanking trabecular bone up to 1 mm deep into PCL and 99-PCL pores, but this osseous integration was sporadic and not seen in all scaffolds. There were 2 requirements for woven bone integration: firstly, deeper scaffold pores needed to contain angiogenic mesenchyme, and secondly, fractured trabecular bone must regenerate right up to the scaffold edge to allow the leading trabecular bone edge to continue regenerating into the pores. These results are still an improvement over previous studies in which bone was observed to regenerate on top of, but not inside of, various implants placed in osteochondral defects in other New Zealand White rabbit models [21–25]. It was previously reported that 99% DDA chitosan or peptide coatings were necessary to promote primary MSC adhesion and calcified matrix formation on the PCL pore surfaces *in vitro* [6–8]. We were

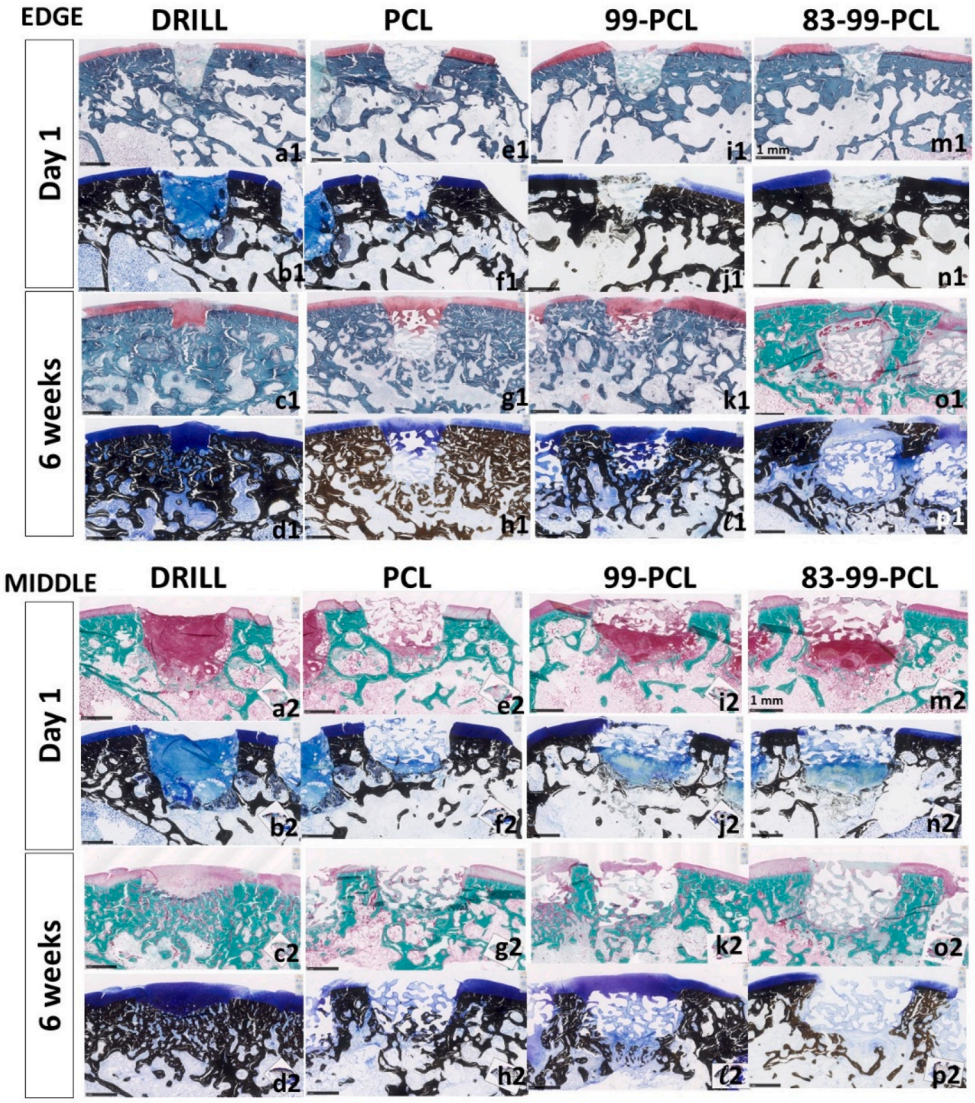

Fig. 5. Nondecalcified histology at the defect edge or middle showing a hematoma filling PCL pores at Day 1 and bone marrow-derived repair tissues filling the pores at 6 weeks post-operative. Panels show (**a-d**) Drill-only, (**e-h**) PCL, (**i-l**) 99-PCL, (**m-p**) 83-99-PCL non-decalcified plastic sections, stained with SafO-fast green (Edge: **a1,c1, e1,g1,i1,k1,m1**), von Kossa/Toluidine blue (edge and middle: **b,d,f,h,j,l,n,p**) or Goldner Trichrome (Edge: **o1**; Middle: **a2,c2,e2, g2,i2,k2,m2,o2**). SafO stains cartilage tissue red, Goldner Trichrome stains bone green and newly deposited bone, blood vessels and cartilage pink/red, von Kossa/Toluidine blue stains mineralized cartilage and bone black, cartilage tissue purple. Scale bar: 1 mm.

therefore surprised by the similar level of woven bone incorporation into PCL and 99-PCL *in vivo*. These results lead us to realize that (1) osteogenesis *in vitro* depends on appositional growth of osteoblasts from a solid artificial substrate, whereas (2) osteogenesis *in vivo* occurred through appositional growth of osteoblasts from remodeling living trabecular bone surfaces into pores already populated with mesenchymal tissues. Osseous integration failed to occur into 83-99-PCL pores at 6 weeks partly because innate immune responses to 83% DDA chitosan led to trabecular bone regression from the scaffold edges. It is possible that with longer repair periods and full resolution of inflammatory cell presence that osteogenesis could proceed in the 83-99-PCL pores. The reaction to 83-99-PCL was different from other studies using nanofibrous structured PCL that induced a foreign body response and suppressed bone ingrowth [11]. In the present study no foreign body giant cells were observed, and the scaffold was not enveloped by capsular fibrous tissues. The scaffolds permitted normal spontaneous regenerative responses that were however different from endogenous repair because the woven bone that infiltrated into PCL pores was growing into tissue mesenchyme instead of calcified cartilage.

Comparable levels of mineralized tissue formed in our cell-free PCL and 99-PCL scaffolds (6.8%, 10.3% BV/TV after 6 weeks), and in a nude mouse orthotopic model with 350–800 μm pore size PCL seeded with BMP-7 expressing gingival fibroblasts (7.2%–10.3% BV/TV after 8 weeks) [9]. Jensen et al. [11] found that 300–500 μm pore size PCL implanted in porcine calvarial defects regenerated 2.9%–5.8% BV/TV by micro-CT after 8 weeks of repair. When a tantalum mesh with 430 μm or 650 μm pore size was implanted in canine diaphyseal transcortical drill holes, trabecular bone grew as slender spicules from existing bone into the middle of the pores that subsequently filled in the pore space over 52 weeks of repair [15]. No chondrogenesis was reported in a cortical bone drill hole fracture site [15]. A similar spicule-shaped trabecular bone ingrowth was seen at the base of the PCL and 99-PCL scaffolds in this study. Some trabecular bone ingrowth was free from the pore surfaces while other trabecular bone structures were fused to the PCL surfaces. Blood vessels were always detected in tissues deeper in the pores, towards which the trabecular spicules were growing. These observations support the notion that trabecular bone grows towards soluble signals of unknown character, from inside the pores. These signals could arise from blood vessels (oxygen gradients) [45–47], "founder cells" inside the pore middle, or other sources such as synovial fluid in the model used in this study. Failed osteogenesis could be due to lack of these signals, physical impediments (fibrosis, bone debris), lack of vascular ingrowth, or lack of healthy remodeling trabecular bone surrounding the scaffold perimeter. Future efforts will focus on identifying factors that drive trabecular bone appositional growth.

The role of fracture hematoma in bone regeneration is acknowledged [48–50] yet little information is available on scaffold-hematoma interactions that initiate osteogenic repair. Our PCL scaffolds were

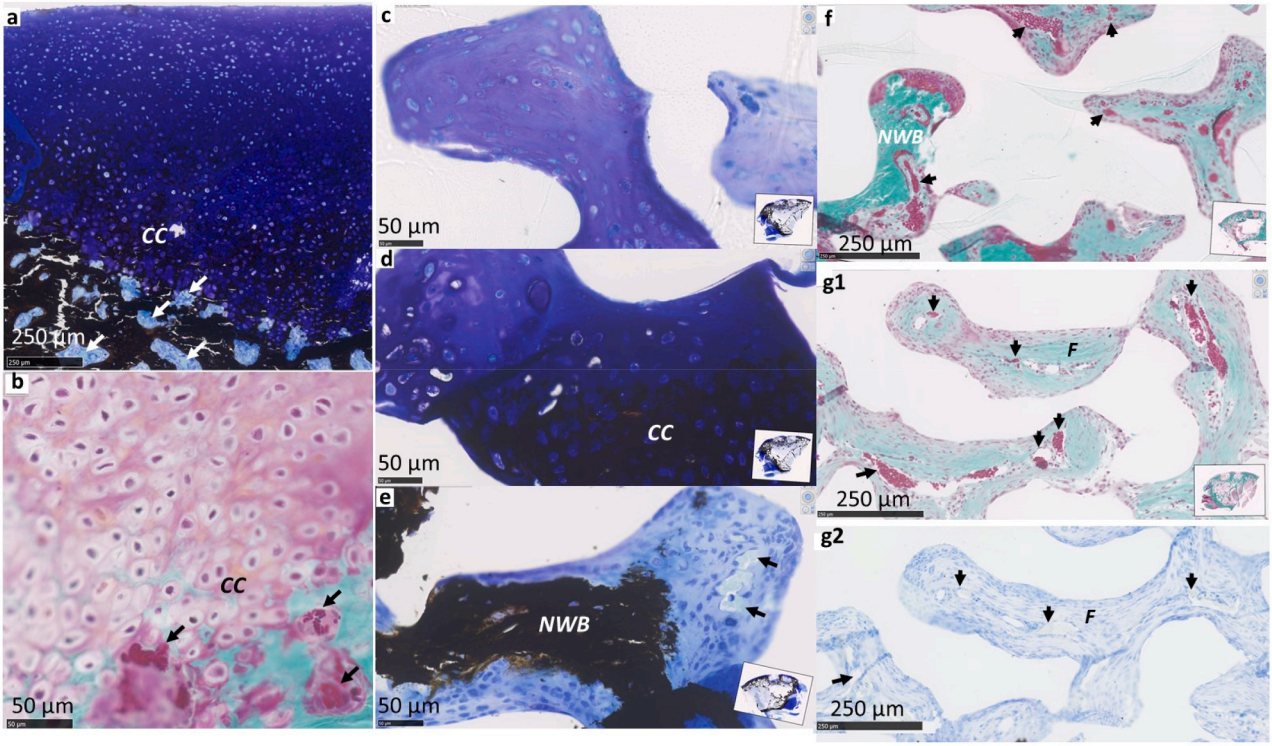

Fig. 6. High-magnification histology of representative 6 week subchondral repair tissues stained with Toluidine blue-von Kossa (**a,c,d,e,g2**) or Goldner trichrome (**b, f,g1**). Drill-only defects (**a-b**) were undergoing endochondral ossification where bone and blood vessels invade calcifying cartilage. Scaffold pore tissues, here shown for 99-PCL, included (**c**) cartilage, (**d**) calcifying cartilage (*CC*), and (**e-f**) vascular new woven bone (*NWB)* or unmineralized angiogenic tissue. Angiogenic blood vessels in 83–99-PCL were often enveloped in fibrous tissue (*F,* in panels **g1-g2**). Symbols: *Arrows: blood vessels. CC: calcified cartilage; NWB: new woven bone. F: fibrous tissue.* Scale bars: (**a,f,g1,g2**) 250 μm, (**b,c,d,e**) 50 μm.

designed with 155 μm pores, above the 100 μm minimum pore size recommended by Hulbert and colleagues for osseous integration of permanent ceramic implants [16]. Using a layer-by-layer approach to coat PCL scaffold pores with chitosan we were able to induce inflammatory cell migration into a porous PCL scaffold coated with 83% DDA chitosan. We observed phagocytosis of both chitosan coatings *in vitro* and *in vivo*, a novel observation permitted by our use of structurally-tuned RITC-chitosans, that was not possible in previous studies by others using non-fluorescent chitosan-coated scaffolds [6,51,52]. Our study was limited by using fluorescent chitosan tracers only at day 1 and not at 6 weeks. We are therefore unable to verify whether some cell adhesion was mediated by polyelectrolyte LbL surfaces. The polyelectrolytes used in this study are not approved for use in humans and more work is needed to identify a clinically suitable LbL method, such as hyaluronic acid-chitosan multilayers [53], to coat the pore surfaces.

Our study was limited by a small number of biological replicates, slight differences in the implant position in the drill hole relative to the cartilage-bone junction, and on-going repair at the 6 week endpoint. Mechanical shear forces created by joint locomotion had a variable and uncontrolled effect on scaffold resurfacing and a scaffold shape anatomically curved to the shape of the trochlear groove may have improved the cartilage repair over the scaffolds (Fig. 9). 99-PCL was covered with more hyaline-like repair cartilage than PCL, suggesting that the chitosan coating permitted better cell adhesion and resistance to shear forces. Current data suggest that chondroinduction cannot take place with local inflammation, and that cartilage resurfacing requires a "quiet" knee joint environment. Knee inflammation is an important but neglected variable that was not reported in other cartilage repair studies using PCL scaffolds [23–25]. Poor osteogenesis and chondrogenesis in untreated control drill hole defects in these prior studies [23–25,54] could be explained by persisting post-operative knee inflammation. It was previously shown that endochondral ossification is inhibited in rabbit knees with a cumulative knee effusion score over 20 [20].

5. Conclusions

PCL scaffolds of 155 μm pore size elicited spontaneous avascular mesenchyme and chondrogenesis, or angiogenic mesenchyme and osteogenesis up to 1 mm deep into the scaffold. Subchondral chondrogenesis and hyaline-like cartilage resurfacing was promoted by 99% DDA chitosan coating. We also report the novel finding that cartilage resurfacing can take place from bone marrow tissues migrating through pores and over the articular scaffold surface, compared to other studies where cartilage was formed from bone plate regenerating over the implant (bone-derived chondroinduction). Our results are an improvement over previously tested cell-free BTE scaffolds for cartilage repair because the scaffold pores were infiltrated by both vascular woven bone and calcifying cartilage tissues. Untreated drill holes however had significantly better ossification and hyaline cartilage resurfacing compared to scaffold-treated defects, therefore future studies should look for a larger pore size with a faster degrading material along with additional biological signals towards identifying the ideal BTE repair device.

CRediT authorship contribution statement

Caroline D. Hoemann: Conceptualization, Methodology, Validation, Formal analysis, Investigation, Resources, Writing – original draft, Writing – review &; editing, Visualization, Supervision, Project administration, Funding acquisition (CIHR, FRQS-RSBO, GMU). **Javier Rodríguez González:** Methodology, Investigation, Visualization, Writing – review & editing. **Jessica Guzmán-Morales:** Methodology, Validation, Formal analysis, Visualization, Investigation, Writing –

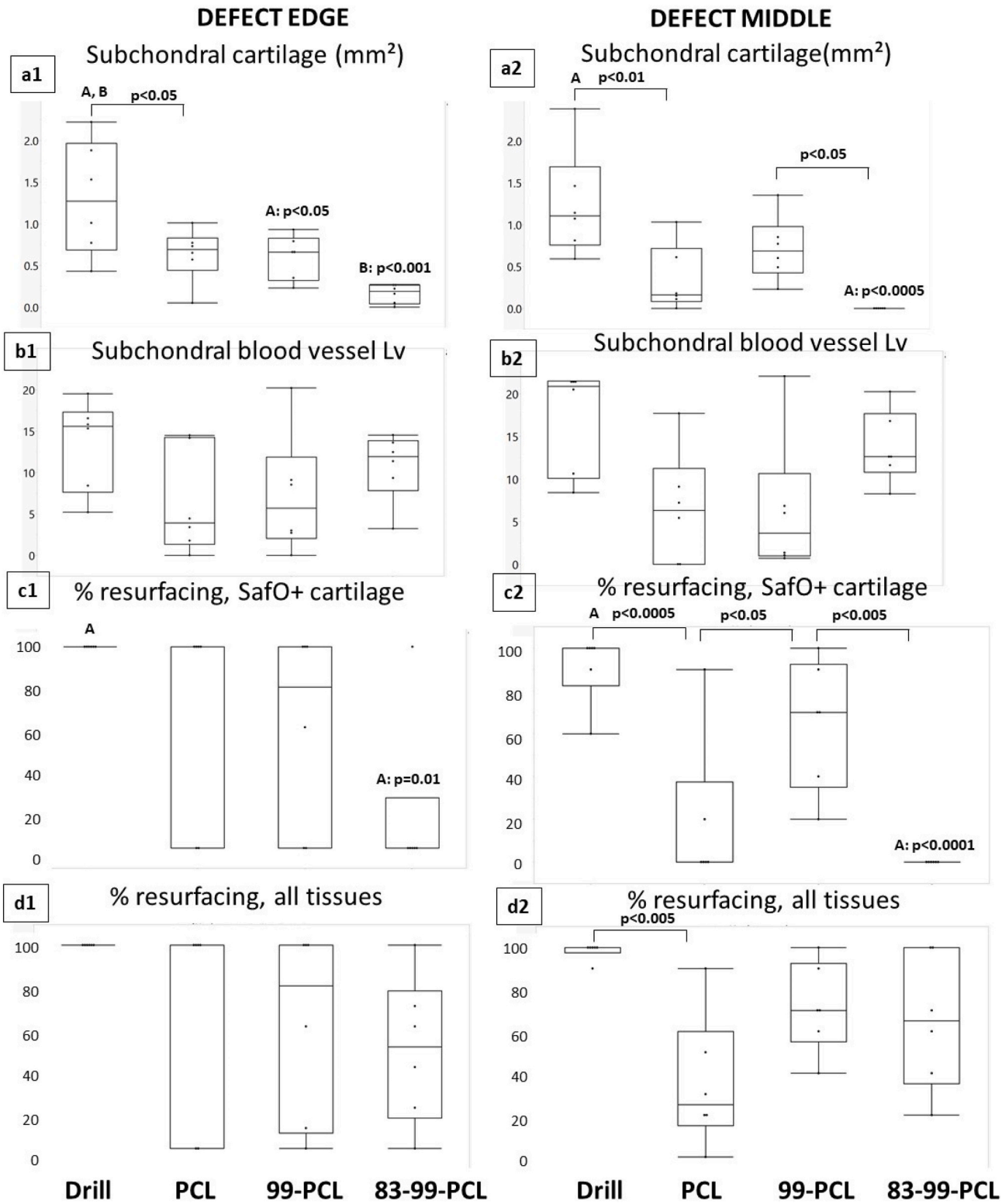

Fig. 7. Histomorphometry of subchondral (a1-a2) cartilage infiltration, (b1-b2) blood vessel stereology of angiogenesis (vessels/mm^2), and % defect resurfacing with (c1-c2) Safranin O+ cartilage or (d1-d2) all soft repair tissue from transverse sections near the defect edge (a1-d1) and middle (a2-d2). Graphs show individual data points (dots), median (horizontal line), interquartile range (box) and min-max (whiskers), N = 6.

review & editing. **Gaoping Chen:** Methodology, Investigation. **Ebrahim Jalali Dil:** Methodology, Investigation, Formal analysis. **Basil D. Favis:** Conceptualization, Validation, Writing – review & editing, Supervision, Funding acquisition (FRQS-RSBO). Manuscript approval: all authors.

Declaration of competing interest

The authors declare the following financial interests/personal relationships which may be considered as potential competing interests: C. D. Hoemann: ORTHO RTi: Scientific Advisory Board, shareholder. J.

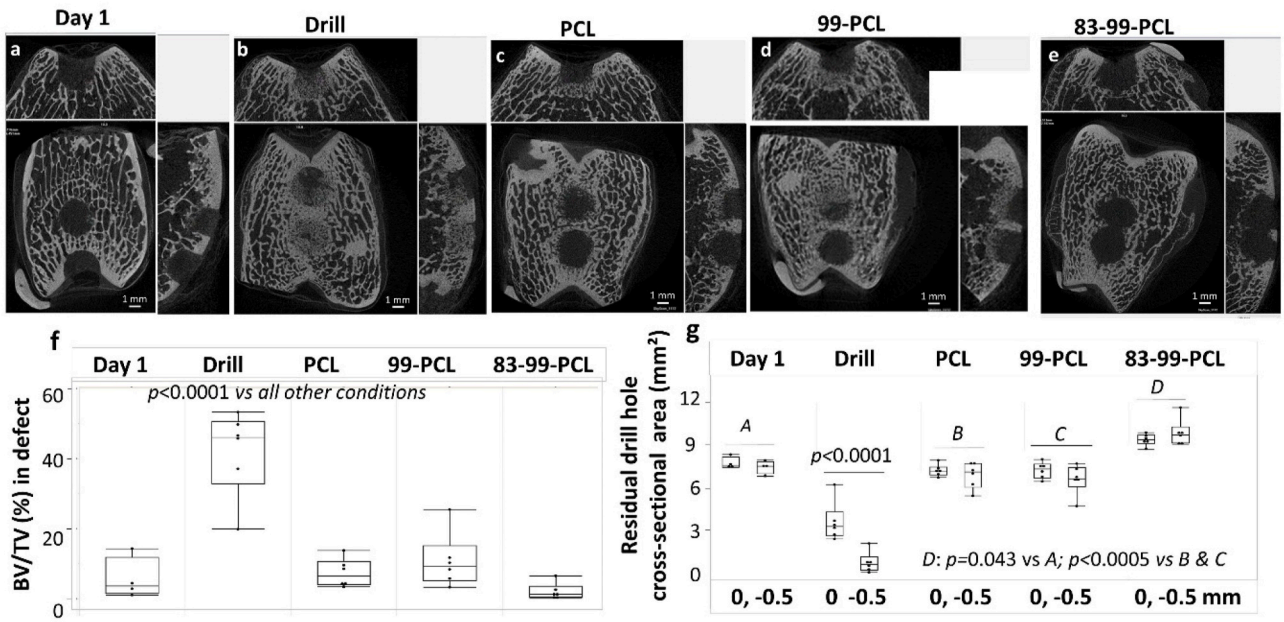

Fig. 8. Example micro-CT images of mineralized tissue formation in microdrill defects at day 1 (a) and 6 weeks (b-e, conditions as indicated), (f) measures of bone volume fraction (%) in a 3 mm diameter 2 mm deep volume of interest, and (g) residual drill hole area (mm^2) at the drill hole top and −0.5 mm below the chondral-osseous junction (labeled as 0, -0.5 mm, panel g). Graphs show individual data points (dots), median (horizontal line), interquartile range (box) and min-max (whiskers), N = 6. Scale bar: 1 mm.

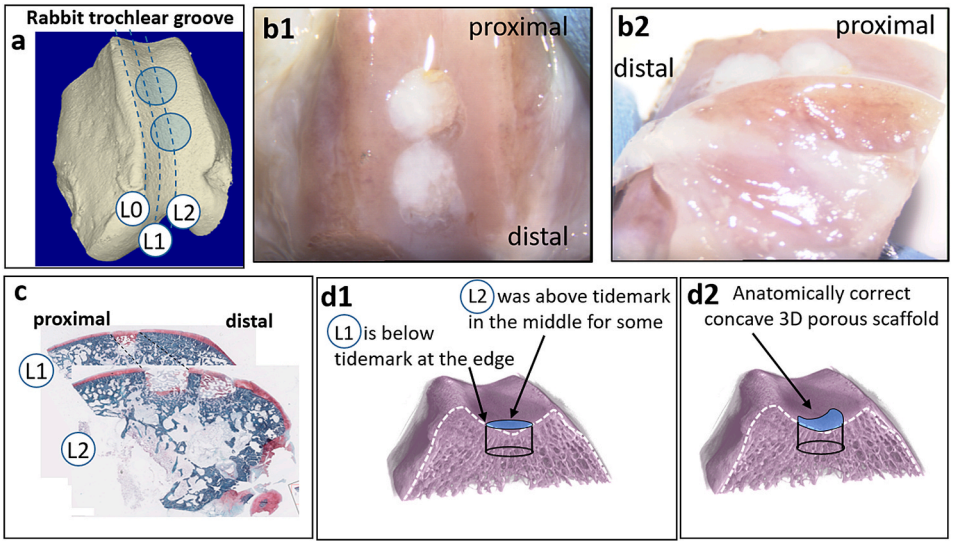

Fig. 9. Diminished resurfacing over some proximal defects was potentially due the curvature of the trochlea and thinner cartilage that led to greater shear forces in the middle of the scaffold, as illustrated through (a) 3-D micro-CT of a rabbit distal femur and sagittal histology sections collected in this study, (b1-b2) macroscopic images of repaired drill holes, (c) serial sagittal sections, and (d1-d2) transverse view of the trochlear groove. Trochlear cartilage is thinner in the proximal area than the distal area, suggesting that shear forces on the flat scaffold that occasionally reached above the tidemark may have been greater in the proximal sites and rubbed off some early mesenchymal tissues growing out and over the pores. A concave scaffold design (d2) would better accommodate shear forces. L0: outside the defect area. L1: edge sagittal section. L2: middle sagittal section.

Guzmán-Morales: ORTHO RTi: shareholder. G. Chen: ORTHO RTi: shareholder. All other authors: no known competing financial interests.

Acknowledgments

Funding sources: Fonds de la Recherche Quebec-Sante, RSBO Grant R0020293; Canadian Institutes of Health Research (CIHR) Operating

grant 313615; George Mason University start-up funds. We are grateful for the valuable contributions of Janet Henderson, Viorica Lascau, Julie Tremblay, Jun Sun, Geneviève Picard, Sara Hosseini, Tess Berthier, and Geoffrey Li to this project.

Appendix A. Supplementary data

Supplementary data to this article can be found online at https://doi.org/10.1016/j.bioactmat.2021.09.012.

References

[1] D.W. Hutmacher, Scaffolds in tissue engineering bone and cartilage, Biomaterials 21 (2000) 2529–2543.
[2] N. Abbasi, S. Hamlet, R.M. Love, et al., Porous scaffolds for bone regeneration, J. Sci.: Advanced Materials and Devices 5 (2020) 1–9.
[3] D.W. Hutmacher, T. Schantz, I. Zein, et al., Mechanical properties and cell cultural response of polycaprolactone scaffolds designed and fabricated via fused deposition modeling, J. Biomed. Mater. Res. 55 (2001) 203–216.
[4] Q.P. Pham, U. Sharma, A.G. Mikos, Electrospun poly(ε-caprolactone) microfiber and multilayer nanofiber/microfiber scaffolds: characterization of scaffolds and measurement of cellular infiltration, Biomacromolecules 7 (2006) 2796–2805.
[5] H. Zhang, C.-Y. Lin, S.J. Hollister, The interaction between bone marrow stromal cells and RGD-modified three-dimensional porous polycaprolactone scaffolds, Biomaterials 30 (2009) 4063–4069.
[6] Z. Yang, Y. Wu, C. Li, et al., Improved mesenchymal stem cells attachment and *in vitro* cartilage tissue formation on chitosan-modified Poly(L-Lactide-*co*-Epsilon-Caprolactone) scaffold, Tissue Eng. 18 (2012) 242–251.
[7] N. Ghavidel Mehr, X. Li, G. Chen, et al., Pore size and LbL chitosan coating influence mesenchymal stem cell in vitro fibrosis and biomineralization in 3D porous poly(ε-caprolactone) scaffolds, J. Biomed. Mater. Res. 103 (2015) 2449–2459.
[8] X. Li, N. Ghavidel Mehr, J. Guzmán-Morales, et al., Cationic osteogenic peptide P15-CSP coatings promote 3-D osteogenesis in poly(epsilon-caprolactone) scaffolds of distinct pore size, J. Biomed. Mater. Res. 105 (2017) 2171–2181.
[9] S.M.M. Roosa, J.M. Kemppainen, E.N. Moffitt, et al., The pore size of polycaprolactone scaffolds has limited influence on bone regeneration in an in vivo model, J. Biomed. Mater. Res. 92A (2010) 359–368.
[10] A. Ferrand, S. Eap, L. Richert, et al., Osteogenetic properties of electrospun nanofibrous PCL scaffolds equipped with chitosan-based nanoreservoirs of growth factors, Macromol. Biosci. 14 (2014) 45–55.
[11] J. Jensen, J.H.D. Rölfing, D.Q.S. Le, et al., Surface-modified functionalized polycaprolactone scaffolds for bone repair: in vitro and in vivo experiments, J. Biomed. Mater. Res. 102 (2014) 2993–3003.
[12] T.C. Lim, K.S. Chian, K.F. Leong, Cryogenic prototyping of chitosan scaffolds with controlled micro and macro architecture and their effect on in vivo neo-vascularization and cellular infiltration, J. Biomed. Mater. Res. 94A (2010) 1303–1311.
[13] Y. Kuboki, Q. Jin, M. Kikuchi, et al., Geometry of artificial ECM: sizes of pores controlling phenotype expression in BMP-induced osteogenesis and chondrogenesis, Connect. Tissue Res. 43 (2002) 529–534.
[14] J.D. Bobyn, R.M. Pilliar, H.U. Cameron, et al., The optimum pore size for the fixation of porous-surfaced metal implants by the ingrowth of bone, Clin. Orthop. Relat. Res. 150 (1980) 263–270.
[15] J.D. Bobyn, G.J. Stackpool, S.A. Hacking, et al., Characteristics of bone ingrowth and interface mechanics of a new porous tantalum biomaterial, Journal of Bone and Joint Surgery, Br. 81 (1999) 907–914.
[16] S.F. Hulbert, F.A. Young, R.S. Mathews, et al., Potential of ceramic materials as permanently implantable skeletal prostheses, J. Biomed. Mater. Res. 4 (1970) 433–456.
[17] N. Ghavidel Mehr, X. Li, M.B. Ariganello, et al., Poly(ε-caprolactone) scaffolds of highly controlled porosity and interconnectivity derived from co-continuous polymer blends: model bead and cell infiltration behavior, J. Mater. Sci. Mater. Med. 25 (2014) 2083–2093.
[18] N. Ghavidel Mehr, C.D. Hoemann, B.D. Favis, Chitosan surface modification of fully interconnected 3D porous poly(ε-caprolactone) by the LbL approach, Polymer 64 (2015) 112–121.
[19] C.D. Hoemann, H. El-Gabalawy, M.D. McKee, In vitro osteogenesis assays: influence of the primary cell source on alkaline phosphatase activity and mineralization, Pathol. Biol. 57 (2009) 318–323.
[20] J. Guzmán-Morales, C.-H. Lafantaisie-Favreau, G. Chen, et al., Subchondral chitosan/blood implant-guided bone plate resorption and woven bone repair is coupled to hyaline cartilage regeneration from microdrill holes in aged rabbit knees, Osteoarthritis Cartilage 22 (2014) 323–333.
[21] M. Yokota, K. Yasuda, N. Kitamura, et al., Spontaneous hyaline cartilage regeneration can be induced in an osteochondral defect created in the femoral condyle using a novel double-network hydrogel, BMC Muscoskel. Disord. 12 (2011) 49.
[22] T.A. Holland, E.W.H. Bodde, L.S. Baggett, et al., Osteochondral repair in the rabbit model utilizing bilayered, degradable oligo(poly(ethylene glycol) fumarate) hydrogel scaffolds, J. Biomed. Mater. Res. 75 (2005) 156–167.
[23] P. Duan, Z. Pan, L. Cao, et al., The effects of pore size in bilayered poly(lactide-co-glycolide) scaffolds on restoring osteochondral defects in rabbits, J. Biomed. Mater. Res. 102 (2014) 180–192.
[24] Z. Pan, P. Duan, X. Liu, et al., Effect of porosities of bilayered porous scaffolds on spontaneous osteochondral repair in cartilage tissue engineering, Regen Biomater 2 (2015) 9–19.
[25] W. Zhang, Q. Lian, D. Li, et al., Cartilage repair and subchondral bone migration using 3D printing osteochondral composites: a one-year-period study in rabbit trochlea, BioMed Res. Int. 2014 (2014) 1–16.
[26] J. Rouwkema, N.C. Rivron, C.A. van Blitterswijk, Vascularization in tissue engineering, Trends Biotechnol. 26 (2008) 434–441.
[27] Á.E. Mercado-Pagán, A.M. Stahl, Y. Shanjani, et al., Vascularization in bone tissue engineering constructs, Ann. Biomed. Eng. 43 (2015) 718–729.
[28] D. Fong, P. Grégoire-Gélinas, A.P. Cheng, et al., Lysosomal rupture induced by structurally distinct chitosans either promotes a type 1 IFN response or activates the inflammasome in macrophages, Biomaterials 129 (2017) 127–138.
[29] C.D. Hoemann, D. Fong, Chapter 3: Immunological responses to chitosan for biomedical applications, in: J.A. Jennings, J.D. Bumgardner (Eds.), Chitosan based Biomaterials, vol. 1, Woodhead Publishing, 2017, pp. 45–79.
[30] P. Simard, H. Galarneau, S. Marois, et al., Neutrophils exhibit distinct phenotypes toward chitosans with different degrees of deacetylation: implications for cartilage repair, Arthritis Res. Ther. 11 (2009) R74.
[31] C.-H. Lafantaisie-Favreau, J. Guzmán-Morales, J. Sun, et al., Subchondral pre-solidified chitosan/blood implants elicit reproducible early osteochondral wound-repair responses including neutrophil and stromal cell chemotaxis, bone resorption and repair, enhanced repair tissue integration and delayed matrix deposition, BMC Muscoskel. Disord. 14 (2013) 27.
[32] C. Mathieu, A. Chevrier, V. Lascau-Coman, et al., Stereological analysis of subchondral angiogenesis induced by chitosan and coagulation factors in microdrilled articular cartilage defects, Osteoarthritis Cartilage 21 (2013) 849–859.
[33] O. Ma, M. Lavertu, J. Sun, et al., Precise derivatization of structurally distinct chitosans with rhodamine B isothiocyanate, Carbohydr. Polym. 72 (2008) 616–624.
[34] C. Kilkenny, W.J. Browne, I.C. Cuthill, et al., Improving bioscience research reporting: the ARRIVE guidelines for reporting animal research, PLoS Biol. 8 (2010), e1000412.
[35] M. Dash, F. Chiellini, R.M. Ottenbrite, et al., Chitosan—a versatile semi-synthetic polymer in biomedical applications, Prog. Polym. Sci. 36 (2011) 981–1014.
[36] S. Méthot, A. Changoor, N. Tran-Khanh, et al., Osteochondral biopsy analysis demonstrates that BST-CarGel treatment improves structural and cellular characteristics of cartilage repair tissue compared with microfracture, CARTILAGE 7 (2016) 16–28.
[37] A. Sarasam, S.V. Madihally, Characterization of chitosan–polycaprolactone blends for tissue engineering applications, Biomaterials 26 (2005) 5500–5508.
[38] L.H. Chong, N.Z. Zarith, N. Sultana, Poly(Caprolactone)/chitosan-based scaffold using freeze drying technique for bone tissue engineering application, in: 2015 10th Asian Control Conference (ASCC), 2015, pp. 1–4.
[39] A. Chevrier, C.D. Hoemann, J. Sun, et al., Chitosan–glycerol phosphate/blood implants increase cell recruitment, transient vascularization and subchondral bone remodeling in drilled cartilage defects, Osteoarthritis Cartilage 15 (2007) 316–327.
[40] N. Thuaksuban, T. Nuntanaranont, S. Suttapreyasri, et al., Repairing calvarial defects with biodegradable polycaprolactone–chitosan scaffolds fabricated using the melt stretching and multilayer deposition technique, BME 25 (2015) 347–360.
[41] K. Tomihata, Y. Ikada, In vitro and in vivo degradation of films of chitin and its deacetylated derivatives, Biomaterials 18 (1997) 567–575.
[42] C.J. Park, N.P. Gabrielson, D.W. Pack, et al., The effect of chitosan on the migration of neutrophil-like HL60 cells, mediated by IL-8, Biomaterials 30 (2009) 436–444.
[43] G. Chen, J. Sun, V. Lascau-Coman, et al., Acute osteoclast activity following subchondral drilling is promoted by chitosan and associated with improved cartilage repair tissue integration, CARTILAGE 2 (2011) 173–185.
[44] C.D. Hoemann, J. Sun, A. Légaré, et al., Tissue engineering of cartilage using an injectable and adhesive chitosan-based cell-delivery vehicle, Osteoarthritis Cartilage 13 (2005) 318–329.
[45] B. Berse, J.A. Hunt, R.J. Diegel, et al., Hypoxia augments cytokine (transforming growth factor-beta (TGF-b) and IL-1)- induced vascular endothelial growth factor secretion by human synovial fibroblasts, Clin. Exp. Immunol. 115 (1999) 176–182.
[46] D.J. Ceradini, A.R. Kulkarni, M.J. Callaghan, et al., Progenitor cell trafficking is regulated by hypoxic gradients through HIF-1 induction of SDF-1, Nat. Med. 10 (2004) 858–864.
[47] A. Di Luca, B. Ostrowska, I. Lorenzo-Moldero, et al., Gradients in pore size enhance the osteogenic differentiation of human mesenchymal stromal cells in three-dimensional scaffolds, Sci. Rep. 6 (2016) 22898.
[48] H.T. Shiu, B. Goss, C. Lutton, et al., Formation of blood clot on biomaterial implants influences bone healing, Tissue Eng. B Rev. 20 (2014) 697–712.
[49] H.T. Shiu, P.C. Leung, C.H. Ko, The roles of cellular and molecular components of a hematoma at early stage of bone healing, Journal of Tissue Engineering and Regenerative Medicine 12 (2018) e1911–e1925.
[50] K. Schmidt-Bleek, H. Schell, P. Kolar, et al., Cellular composition of the initial fracture hematoma compared to a muscle hematoma: a study in sheep, J. Orthop. Res. 27 (2009) 1147–1151.
[51] S.G. Santos, M. Lamghari, C.R. Almeida, et al., Adsorbed fibrinogen leads to improved bone regeneration and correlates with differences in the systemic immune response, Acta Biomater. 9 (2013) 7209–7217.
[52] J.M. Oliveira, R.A. Sousa, N. Kotobuki, et al., The osteogenic differentiation of rat bone marrow stromal cells cultured with dexamethasone-loaded

carboxymethylchitosan/poly(amidoamine) dendrimer nanoparticles, Biomaterials 30 (2009) 804–813.
[53] B. Thierry, F.M. Winnik, Y. Merhi, et al., Bioactive coatings of endovascular stents based on polyelectrolyte multilayers, Biomacromolecules 4 (2003) 1564–1571.
[54] C. Deng, H. Zhu, J. Li, et al., Bioactive scaffolds for regeneration of cartilage and subchondral bone interface, Theranostics 8 (2018) 1940–1955.